Multi-sensor inline measurements of crystal size and shape distributions during high shear wet milling of crystal slurries

14 authors, including:

Okpeafoh Stephen Agimelen
HSBC
11 PUBLICATIONS **94** CITATIONS

SEE PROFILE

Vaclav Svoboda
University of Strathclyde
6 PUBLICATIONS **29** CITATIONS

SEE PROFILE

Javier Cardona
University of Strathclyde
11 PUBLICATIONS **50** CITATIONS

SEE PROFILE

Some of the authors of this publication are also working on these related projects:

Project   A structural databbase for salt selection (thesis) View project

Project   Intelligent decision support platform for crystallisation processes and particle attributes View project

Original Research Paper

Multi-sensor inline measurements of crystal size and shape distributions during high shear wet milling of crystal slurries

Okpeafoh S. Agimelen [a,*], Vaclav Svoboda [a], Bilal Ahmed [b], Javier Cardona [c], Jerzy Dziewierz [d], Cameron J. Brown [b], Thomas McGlone [b], Alison Cleary [c], Christos Tachtatzis [c], Craig Michie [c], Alastair J. Florence [b], Ivan Andonovic [c], Anthony J. Mulholland [e], Jan Sefcik [a,*]

[a] EPSRC Future Manufacturing Hub for Continuous Manufacturing and Advanced Crystallisation, Department of Chemical and Process Engineering, University of Strathclyde, James Weir Building, 75 Montrose Street, Glasgow G1 1XJ, United Kingdom
[b] EPSRC Future Manufacturing Hub for Continuous Manufacturing and Advanced Crystallisation, Strathclyde Institute of Pharmacy and Biomedical Sciences, Technology and Innovation Centre, University of Strathclyde, 99 George Street, Glasgow G1 1RD, United Kingdom
[c] Centre for Intelligent Dynamic Communications, Department of Electronic and Electrical Engineering, University Of Strathclyde, Royal College Building, 204 George Street, Glasgow G1 1XW, United Kingdom
[d] The Centre for Ultrasonic Engineering, Department of Electronic and Electrical Engineering, University Of Strathclyde, Royal College Building, 204 George Street, Glasgow G1 1XW, United Kingdom
[e] Department of Mathematics and Statistics, University of Strathclyde, Livingstone Tower, 26 Richmond Street, Glasgow G1 1XH, United Kingdom

ABSTRACT

Size and shape distributions are among critical quality attributes of particulate products and their inline measurement is crucial for monitoring and control of particle manufacturing processes. This requires advanced tools that can estimate particle size and shape distributions from multi-sensor data captured in situ across various processing steps.

In this work, we study changes in size and shape distributions, as well as number of particles during high shear wet milling, which is increasingly being employed for size reduction in crystalline slurries in pharmaceutical processing. Saturated suspensions of benzoic acid, paracetamol and metformin hydrochloride were used in this study. We employ our recently developed tools for estimating particle aspect ratio and particle size distributions from chord length distribution (CLD) measurements and imaging. We also compare estimated particle size distributions from CLD and imaging with corresponding estimates from offline instruments.

The results show that these tools are capable of quantitatively capturing changes in particle sizes and shape during wet milling inline. This is the first time that such a capability has been reported in the literature. The ability to quantitatively monitor particle size and shape distributions in real time will enable development of more realistic and accurate population balance models of wet milling and crystallisation, and aid more efficient control of crystallisation processes.

Crown Copyright © 2018 The Society of Powder Technology Japan. Published by Elsevier B.V. This is an open access article under the CC BY license (http://creativecommons.org/licenses/by/4.0/).

1. Introduction

Quantitative particle attributes such as particle size and shape influence behaviours of slurries and powders such as flowability, filterability and dissolution. These behaviours in turn determine performance of various downstream operations carried out in the manufacturing process as well as performance of resulting particulate products. Hence it is necessary that the particles possess the desired particle size distribution (PSD) and shape for a particular process or product application [1–3].

Crystallisation is a widely used separation and purification technique and it is routinely employed in pharmaceutical manufacturing [4]. Outcomes of a crystallisation process in terms of particle size and shape distributions are determined by a complex interplay of nucleation, growth, agglomeration and breakage and can vary widely from batch to batch or when input conditions or process parameters are changed. There are several approaches providing empirical control of particle size distributions (PSD) in crystallisation processes, such as seeding (to provide control over particle number concentrations) [4] and high shear wet milling (to provide control over particle size). In particular, high shear wet milling is a size reduction technique increasingly used in pharmaceutical processing to adjust size and shape distributions in

crystal slurries or generate small particles for effective seeding of subsequent crystallisation steps [5–14].

Adi et al. [5] combined wet milling and wet sieving to produce crystalline particles with a narrow PSD. Particle size analysis was carried out using an offline laser diffraction instrument. Wilson et al. combined wet milling and temperature cycling to adjust the size and shape of needle-like particles [15]. Particle size and shape measurements was carried out using an offline imaging instrument. Yang et al. [8,10,12] used wet milling both to generate seed particles and as a size reduction method for different crystallisation processes. The processes were monitored by inline sensors including the focused beam reflectance measurement (FBRM) [16]. This measurement provides a chord length distribution (CLD) for particles in suspension. The CLD is related to the size and shape of the particles in suspension [16]. The total counts of measured CLDs has been used as an indication for number of particles, while the mean square weighted chord length has been used as an indication of particle size [8,10,12].

Even though CLD total counts are related to number of particles, it is not straightforward to determine the actual number density of particles in a slurry from CLD counts. Similarly, while CLD is related to the PSD, it does not provide an actual PSD of particles. This is because each particle with a given size and shape produces a unique chord length distribution [16] and these are then convoluted in an average weighted by a characteristic particle size to provide an overall CLD for the whole ensemble of particles of different sizes and shapes present in a slurry [17].

Instead of using the mean square weighted chord length as an estimate for the mean particle size, it would be more realistic and accurate to use an actual PSD determined from inline measurements. For example, from transformation of CLD data [18,19] obtained inline or from analysis of inline images [20]. Hence, experimental wet milling studies could then benefit from the estimated particle size and shape distributions. Consider the case of needle-like particles undergo wet milling, their length is likely to be reduced while their width would be much less affected. However, the most probable chord length for a needle-like particle is the width of the particle [21] and so the change in particle length may not be well reflected in the mean square weighted chord length. But this mean square weighted chord length is currently used as an indication for particle size even when needle-like particles are involved [12]. Furthermore, if the PSD is estimated from data captured with inline instruments, there will be no need to sample the slurry for offline estimates of the PSD.

In this work, we implement our recently developed computational tools, CLDInversionApp [22] and ImagingApp [23], in order to quantitatively investigate changes in PSD and particle shape during wet milling when the mill rotational speed is varied. The PSDs are estimated separately from CLD and from imaging data obtained by the inline FBRM and particle vision and measurement (PVM) sensors, respectively. As the PSD is estimated from data captured by inline sensors, the computational tools enable us to monitor changes in particle properties during the wet milling in real time. We also introduce a new method for estimating the number of particles in slurries from the estimated volume based PSD from inline instruments. We analyse inconsistencies arising between PSDs estimated from inline and offline instruments for the same wet milling process, and discuss limitations of inline sensors encountered during the study.

2. Methods

2.1. Materials

The following materials were used in this work: paracetamol (> 98% USP), benzoic acid (> 99.5%), and metformin hydrochloride (reagent grade). Paracetamol and benzoic acid were purchased from Sigma-Aldrich and metformin hydrochloride was purchased from Molekula. The benzoic acid particles were suspended in distilled water obtained from an in-house purification system, and the surfactant Tween 20 from Sigma-Aldrich was added to the benzoic acid slurry to ease dispersion of the particles and avoid foaming. Paracetamol and metformin hydrochloride were suspended in 2-propanol (reagent grade, CAS: 67–63-0, Assay (GLC) > 99.5%) obtained from Fisher Scientific, UK.

2.2. Equipment

The experiments were conducted in a closed loop setup consisting of a Mettler Toledo OptiMax Workstation, a Watson Marlow Du520 peristaltic pump and an IKA MagicLab (module UTL) rotor stator wet mill. The OptiMax workstation consists of a 1L stirred tank crystalliser, which was equipped with an inline Hastelloy Pt100 temperature sensor, PVM and FBRM sensors for monitoring. A sketch of the setup is shown in Fig. 1.

The rubber tubing used in the flow loop had an inner diameter of 3.2 mm, the lengths of the pieces of tubing connecting the 1L stirred tank to the wet mill, the wet mill to the peristaltic pump and the peristaltic pump to the 1L stirred tank were 94.5 cm, 55 cm and 124 cm respectively. The internal volume of the wet mill was 30 mL. The peristaltic pump was operated at 50 rpm corresponding to a volumetric flow rate of 350 mL/min. This then corresponds to a residence time of 5 s of the slurry in the wet mill.

The temperature of the outlet of the wet mill was monitored with a thermometer attached to it. The outlet temperature was controlled to match the temperature of the inlet flow to the wet mill by means of a Lauda heater/chiller connected to the wet mill as shown in Fig. 1. The process conditions of temperature and stirring speed of the slurry in the Workstation were controlled using the iControl v5.2 software from Mettler Toledo.

Data related to the size and the shape of the particles in the wet milling processes was captured with the Mettler Toledo FBRM G400 series and PVM V819 sensors within the stirred tank. The
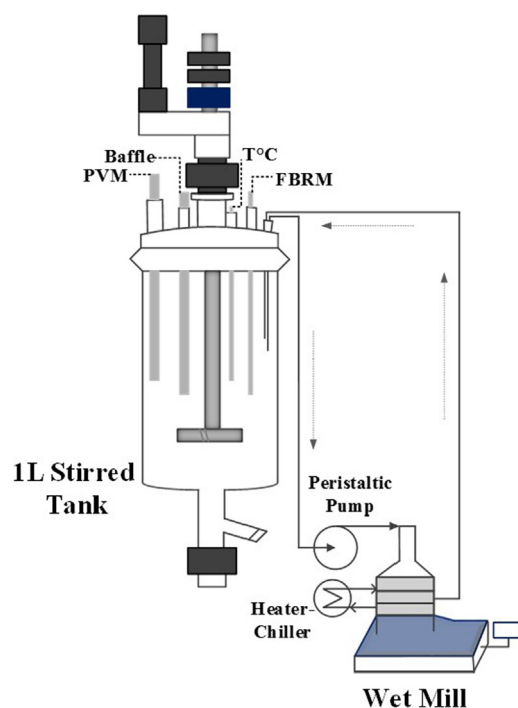

Fig. 1. Sketch of the setup used for the wet milling processes in this study.

FBRM sensor produces a focused laser beam which moves in a circular trajectory. The beam, when incident on a particle, traces out a chord on the particle. The lengths of chords measured over a preset period of time for particles in the slurry is then reported as a CLD [16,18,24,25]. The PVM sensor takes images of the particles using laser beams. The images are recorded on a CCD array which are subsequently transferred to a computer. The size of each image of the PVM V819 is 1360 × 1024 pixels with a pixel size of 0.8 μm [19].

Offline particle size and shape analyses were carried out using the Malvern Morphologi G3 instrument. The Morphologi instrument consists of a dispersion unit which utilises compressed air to disperse the particles over a glass plate. Images of particles on the plate are captured using a camera with a microscope lens. The images are then analysed by the instrument software for size and shape information.

2.3. Experimental procedure

The OptiMax vessel was charged with 900 ml of solvent at 25 °C at the start of each experiment. A predetermined quantity of solid was then added, and heated to 40–50 °C to dissolve. The solution was then cooled to 25 °C over 20 min to saturate. Once the temperature had reached the setpoint value, a predetermined mass of solid powder was added to the saturated solution and allowed to equilibrate for 60 min. Before the addition of the powder, a sample of the original material (starting material) was initially analysed with the offline Morphologi instrument for size and shape information.

After the equilibration period (covering a period T_1), the peristaltic pump and wet mill were started simultaneously. The speed of the pump was maintained at 50 rpm throughout the experiments while that of the wet mill was initially set to 6000 rpm (for a duration T_2) after which it was increased in stages. At the next stage (with duration T_3) of the process, the speed of the wet mill was increased to 10,000 rpm, and subsequently to 14,000 rpm (for a duration T_4) and finally to 18,000 rpm (for a duration T_5). The temperature of the mill outlet was regulated manually by adjusting the heater chiller setpoint in order to maintain it at 25 °C and prevent dissolution. The time intervals T_1 to T_5 varied from 30 to 90 min for each material.

At the end of the time interval T_5, the suspension was filtered and washed in a Buchner funnel. The same solvents which were used in the experiments for benzoic acid and metformin hydrochloride were used for washing each material at the end of their respective experiments, while paracetamol was washed with chilled water. Each material had a low solubility in its respective wash solvent. Each of the cakes obtained at the end of each wet milling process was dried overnight in a vacuum oven. Samples of the milled product obtained at the end of each wet milling process were analysed for size and shape information using the offline Morphologi instrument.

2.3.1. Benzoic acid

Benzoic acid particles were prepared by antisolvent crystallisation (after an initial dissolution of benzoic acid from Sigma-Aldrich) using a mixture of 70–30% ethanol - water mixture as solvent, and 20–80% ethanol - water mixture as antisolvent. A predetermined mass of antisolvent was added at a predetermined rate in order to obtain long needle shaped crystals. The particles were filtered and dried before being suspended in water for the milling experiment. The particles were suspended in water (saturated with benzoic acid) due to the low solubility of benzoic acid in water. However, due to poor wettability of benzoic acid in water, the surfactant Tween 20 was used at a concentration of 2 ml/L. The solid loading was 1.6% w/w.

2.3.2. Paracetamol

Paracetamol from Sigma-Aldrich was dissolved in isoamyl alcohol after which prism like particles were obtained by cooling crystallisation. The particles obtained from the cooling crystallisation were then suspended in a saturated solution of paracetamol in 2-propanol for the wet milling experiment. The solid loading was 4.2% w/w. Although the solubility of paracetamol in 2-propanol is relatively high, the solvent was chosen to avoid agglomeration.

2.3.3. Metformin hydrochloride

Metformin from Molekula was used directly as the particles were already rod-like. The particles were then suspended in a saturated solution of metformin in 2-propanol (in which metformin has a low solubility and good dispersion) for the wet milling process. The solid loading was 3.5% w/w. The wet milling process for metformin was stopped at the stage T_4 (with the mill speed of 14,000 rpm) as the particles were quickly broken in this case.

2.4. Data analysis

As mentioned above, the starting material and the milled product for each material were analysed for size and shape information using the offline Morphologi G3 instrument. The CLD data acquired using the inline FBRM sensor (using the macro mode with no weighting) were analysed using a previously developed inversion algorithm [18,22] which estimates corresponding particle size distribution and aspect ratio (assumed to be same for all particles). Similarly, the images captured using the inline PVM sensor were analysed using a previously developed [19,23] image processing algorithm to obtain projections for particles captured in images and to provide the corresponding particle length and aspect ratio for each particle deemed to be in focus. Therefore, detailed size and shape distributions can be obtained, similar to those from offline measurements.

The number of particles produced during the wet milling process can be determined from an estimated volume based PSD for the particles in the suspension and solid loading (which is constant during wet milling under saturated conditions). To estimate the number of particles, the particle length L is discretised and classified into N bins with the characteristic length $\bar{L}_i = \sqrt{L_i L_{i+1}}$ of bin i representing the length of particles in bin i, where L_i and L_{i+1} are the bin boundaries of bin i. The number of particles N_i in bin i is given as

$$N_i = \frac{\tilde{m}_i M_0}{\rho v_i}. \tag{1}$$

where $\tilde{m}_i$ is the mass fraction of the particles in bin i, M_0 is the mass of the initially suspended particles (which is constant as there is no growth or dissolution), ρ is the density of particles and v_i is the volume of the particles in bin i. Approximating the shape of all particles in each bin with an ellipsoid of semi-major axis length $\bar{a}_i = \bar{L}_i/2$ and two equal semi-minor axis length $\bar{b}_i = \bar{r}_i \bar{a}_i$, where $\bar{r}_i$ is the mean aspect ratio[1] of all the particles in bin i, gives the volume of the particles in bin i as $v_i = \pi \bar{r}_i^2 \bar{L}_i^3/6$. Since all particles have the same density, the mass fraction of the particles in bin i can be replaced by their volume fraction $\tilde{v}_i$. Then the number of particles in bin i becomes

$$N_i = \frac{6 \tilde{v}_i M_0}{\rho \pi \bar{r}_i^2 \bar{L}_i^3}. \tag{2}$$

---

[1] The aspect ratio is defined here as the ratio of width to length of particles.

When the volume based PSD is estimated from CLD inversion [18], the corresponding number of particles $\mathcal{N}_{CLD}$ is obtained by summing over all bins as

$$\mathcal{N}_{CLD} = \sum_{i=1}^{N} N_i. \qquad (3)$$

As the slurry is initially allowed to equilibrate during the stage T_1 of each of the wet milling processes, the number of particles estimated at the stage T_1 will be taken as the base number of particles $\mathcal{N}_{CLD}^0$. Then the number of particles relative to the base number of particles $\widehat{N}_{CLD}$ is obtained from $\widehat{N}_{CLD} = \mathcal{N}_{CLD}/\mathcal{N}_{CLD}^0$.

In the case of image analysis, the mean number of objects per frame $\mathcal{N}_{IMG}$ is used as a measure of the number of particles. It is estimated by counting all objects which were detected and contained wholly within the image frames. This number of objects is then divided by the total number of frames to obtain $\mathcal{N}_{IMG}$. Similar to the case of CLD, the number of particles estimated from images at T_1 will be taken as the base $\mathcal{N}_{IMG}^0$. At the subsequent stages, the number of particles estimated from images relative to the base number of particles $\widehat{N}_{IMG}$ will be obtained from $\widehat{N}_{IMG} = \mathcal{N}_{IMG}/\mathcal{N}_{IMG}^0$.

3. Results and discussions

The three particle analysis techniques employed in this work consistently showed particle breakage during wet milling progressing from the lowest to the highest mill rotational speed. However, the different techniques showed varying sensitivities as process conditions and particle size and shape distributions changed. Below we present and discuss results for benzoic acid in detail and analyse respective limitations of the different techniques using results from all three systems. A complete set of results for paracetamol and metformin are available in the supplementary information.

3.1. Offline analysis

The two-dimensional volume based probability density function (PDF) of particle length and aspect ratio estimated using offline imaging (Morphologi G3) for both the starting material and the final milled product for benzoic acid are shown in Fig. 2(a) and (b), respectively[2]. The data clearly show particle breakage as the broad peak between particle lengths 100 and 1000 microns and aspect ratios from 0.4 to 1 moves towards smaller lengths and higher aspect ratios between Fig. 2(a) and (b). This is indicative of breakage of large elongated particles to much shorter, more isometric ones. In Fig. 2(c) and (d) we show one-dimensional projections of two-dimensional PDFs above, in terms of volume based particle length distributions and aspect ratio distribution for the starting material and the final milled product. Similar results were also obtained for paracetamol and metformin as shown in Figs. 11 and 13 of the supplementary information.

3.2. Analysis of inline CLD data

The total CLD counts at the different time intervals T_1 to T_5 during the wet milling of benzoic acid are shown by the solid line in Fig. 3(a). The increase in total chord counts over the wet milling stages T_1 to T_5 seen in Fig. 3(a) clearly indicates breakage of parti-

cles during the process as the conditions were such that there was no nucleation or growth of particles. This breakage is also reflected in the increase in the relative number of particles $\widehat{N}_{CLD}$ as shown by the symbols in Fig. 3(a).

The mean CLD captured in 5 min time intervals ($\overline{T}_1$ to $\overline{T}_5$ shown by the vertical bars in Fig. 3(a)) within the time intervals T_1 to T_5 are shown by the symbols in Fig. 3(b). Breakage of particles leads to an increase in the counts for smaller chord lengths of these CLDs over the time intervals $\overline{T}_1$ to $\overline{T}_5$ as the CLD acquisition time was fixed throughout the process.

The solid lines (with the colours corresponding to the symbols) in Fig. 3(b) are the fitted CLDs obtained by solving the associated inverse problem. This involves searching for a PSD at different aspect ratios r (all particles are assumed to have the same mean aspect ratio) whose corresponding CLD gives the best fit to the measured CLD [18]. In the case of Fig. 3(b), these best fits were obtained at $r = 0.6$ ($\overline{T}_1$), $r = 0.5$ ($\overline{T}_2$), $r = 0.5$ ($\overline{T}_3$), $r = 0.5$ ($\overline{T}_4$) and $r = 0.8$ ($\overline{T}_5$) as indicated in Fig. 3(b).

The PSDs estimated from the CLDs in Fig. 3(b) (at the best fit values of r) are shown in Fig. 3(c). The estimated PSDs (Fig. 3(c)) both show breakage of particles moving from T_1 to T_5. That is, the peaks of the distributions shift to the left and both the right and left tails of the distributions shift to the left on moving from T_1 to T_5. Similar results were obtained from the analysis of CLD data for paracetamol and metformin. The results are shown in Section 4 of the supplementary information.

3.3. Analysis of inline PVM images

Breakage of benzoic acid particles during wet milling is evident from inspecting inline PVM images. However, image analysis provides quantitative estimates of how particle size and shape distributions vary in response to changing mill rotational speed. This can be clearly seen in the two-dimensional probability density function of particle length and aspect ratio (Fig. 4(a)) obtained from the analysis of PVM images (moving from T_1 to T_5). We note that the particle length distribution obtained from PVM images has lower and upper cut-offs due to limitations of image size, resolution and subsequent image processing. At the lower end, the cut-off is at a length of about 25 μm. This is because of the resolution of PVM images and a choice of a minimum pixel area required (here we used $\lesssim 576$ μm², corresponding to length $\lesssim 24$ μm) by an image processing algorithm to distinguish between relevant objects and background image noise. Hence all particles with smaller lengths were rejected by the image processing algorithm. Also, objects with lengths $\gtrsim 500$ μm tend to be undercounted by the image processing algorithm. This is because larger objects have a higher chance of touching the image frame so that most of them are rejected. Hence, the particle length estimates from PVM images are most reliable within the range from about 25 to about 500 μm [19].

3.4. Limitations of particle sizing techniques

Wet milling of particle slurries from three systems used in this work presented different challenges pertaining to particle sizing techniques and corresponding data analysis as discussed below.

3.4.1. Limitations of offline analysis

One of key limitations of particle sizing using offline imaging, such as the Morphologi G3 used in this work, is the change of state of the particles between the slurry and the dry powder used for analysis. In some cases, particles that were initially agglomerated before suspension could become de-agglomerated upon suspension and agitation. This is particularly obvious in the case of the

---

[2] The raw estimates of particle lengths and widths from the Morphologi instrument was extracted and analysed. In the volume based analysis, the particles were treated as ellipsoids of major axes lengths equal to the originally estimated particle lengths. The two minor axes were set equal to the originally estimated particle widths. This was to make the analysis consistent with those carried out on the inline PVM images and the particle representation in the CLD analysis.
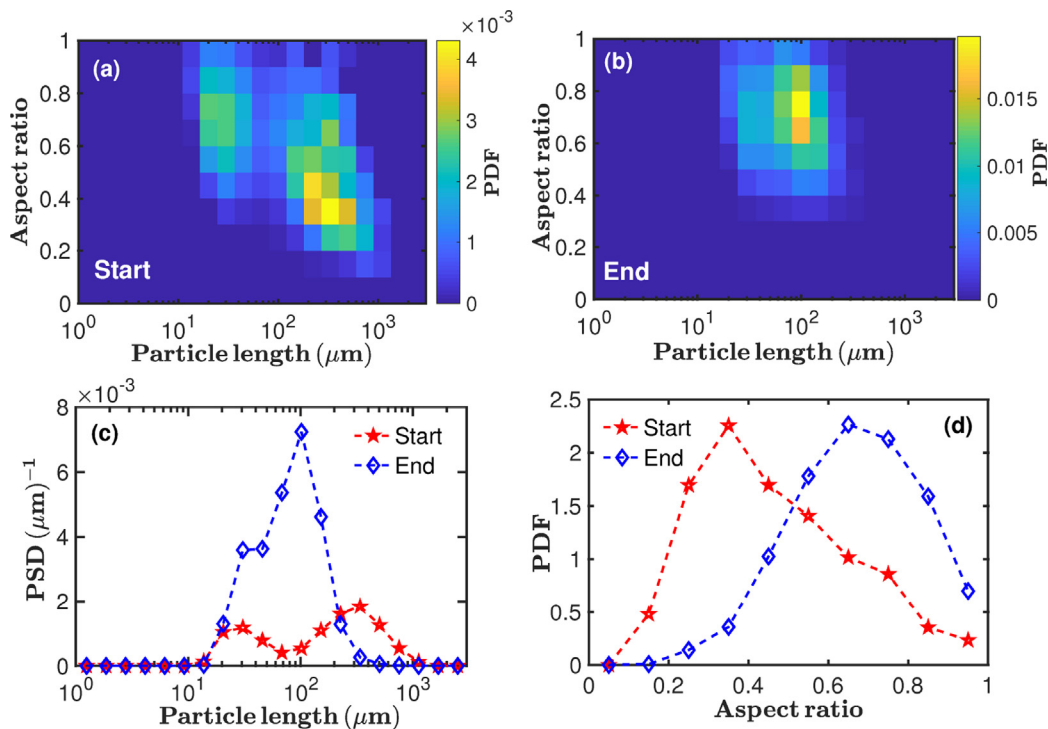
Fig. 2. 2D volume based probability density function (PDF) of particle length and aspect ratio for the starting material (a) and the final milled product (b) for benzoic acid from the offline Morphologi instrument. Corresponding 1D volume based particle length distributions (c) and 1D volume based aspect ratio distributions (d) of the starting material and the final milled product for benzoic acid.
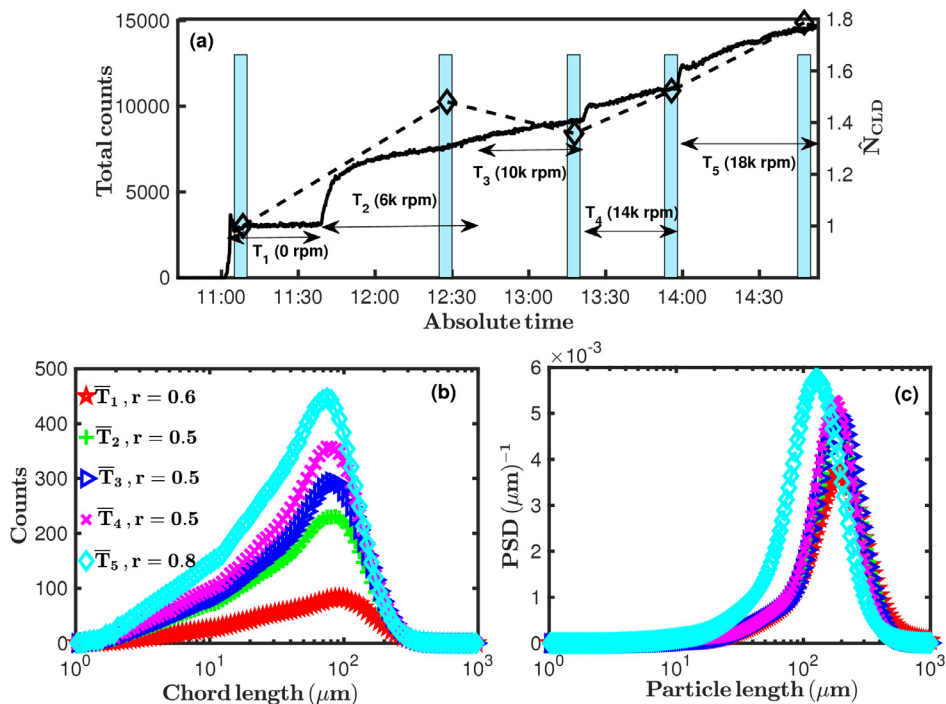

Fig. 3. The total chord length counts for the benzoic acid sample during the wet milling stages covering the time intervals T_1 to T_5 are shown by the solid line in (a), while the symbols show the relative number of particles $\hat{N}_{CLD}$ for the same sample. The mean chord length distributions (CLDs) acquired in the 5 min intervals $\overline{T}_1$ to $\overline{T}_5$ (shown by the vertical bars in (a)) within the stages T_1 to T_5 are shown by the symbols in (b). The solid lines in (b) (with colours corresponding to the symbols) are the estimated CLDs at the aspect ratios r indicated in the Fig. The estimated volume based PSDs from the CLDs shown in (b) at the aspect ratios indicated in (b) are shown in (c). (For interpretation of the references to colour in this figure legend, the reader is referred to the web version of this article.)

paracetamol starting material. The sample images (Fig. 3 of the supplementary information) from the offline instrument suggests the presence of agglomerates up to 1000 μm. Whereas, these large

agglomerates seem to be missing in suspension as suggested by the sample image from the PVM sensor at T_1 in Fig. 8(T_1) of the supplementary information. The presence of the large agglomerates in
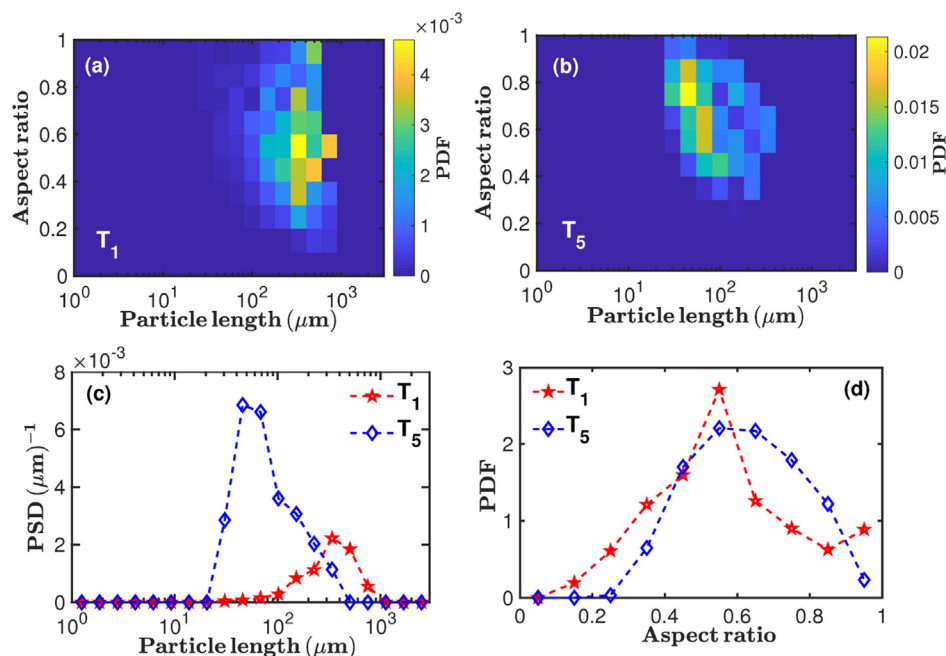
Fig. 4. 2D volume based probability density functions (PDFs) of particle length and aspect ratio estimated from images captured with inline PVM instrument during wet milling stages T_1 (a) and T_5 (b) for benzoic acid. Corresponding 1D volume based particle length distributions (c) and 1D volume based aspect ratio distributions (d) during wet milling stages T_1 and T_5 for benzoic acid.

the starting material of paracetamol leads to the peak close to 1000 μm in the estimated volume based PSD for paracetamol obtained with the Morphologi instrument. This is seen in Fig. 5(b). Hence the peaks of the estimated volume based PSDs from CLD and PVM images at T_1 are shifted to the left of the corresponding estimate of the starting material of paracetamol obtained from the offline Morphologi instrument, as seen in Fig. 5(b).

In some other cases, particles that were initially separated could become agglomerated upon filtration and drying for offline analysis. This is obvious in the case of the milled product of benzoic acid. The sample PVM image (Fig. 7(T_5) of the supplementary information) of the benzoic acid sample suggests that the particles were mostly separated at T_5 while in suspension. However, a significant amount of them had become agglomerated upon filtering and drying before offline analysis with the Morphologi instrument, as seen in Fig. 2 of the supplementary information.

3.4.2. Limitations of CLD analysis

The idealised CLD model [21] used in this work assumes that all particles lie on the focal plane of the laser spot of the FBRM instrument, and that the laser spot makes a straight chord on the particles. However, as the length dimensions of the particles become comparable to the diameter of the circular laser beam (the FBRM G400 used in this work has a diameter of 5.3 mm), the curvature of the chord becomes more pronounced and the relationship between the particle size and shape and the corresponding CLD becomes less accurate as the particle length increases.

This situation particularly arises in the case of the starting material of metformin. The sample image of the starting material of metformin in Fig. 5 of the supplementary information suggests the presence of particles of lengths ≈ 3000 μm. These lengths dimensions are not accurately represented in the CLD data, so that the peak of the volume based PSD estimated from CLD analysis at T_1 is shifted to the left of the corresponding estimate using the offline Morphologi instrument. This is seen in Fig. 5(c). There is also the possibility that some of these long rod-like particles were bro-

ken upon suspension and agitation, so that their contribution to the CLD data is reduced.

Another issue with CLD analysis is the situation where objects are transparent to the laser beam. There was a significant amount of bubbles produced during the wet milling of the benzoic acid sample, as seen in the PVM image in Fig. 7 of the supplementary information. Even though these bubbles are not crystalline particles, they contribute to the chord count of the FBRM sensor. Because the bubbles are transparent to the laser beam, they lead to chord splitting [16,24] at their boundaries. This could lead to an artificially high count of shorter chords, and hence to an over estimation of fines in the estimated volume based PSD from CLD analysis.

The CLD modality is inherently biased towards larger particles [18]. This leads to a situation whereby when there is a significant proportion of larger particles in a suspension, the aspect ratio predicted from CLD analysis becomes biased towards that of the large particles. This is clearly demonstrated in the case of metformin. Analysis of CLD data for metformin suggests an aspect ratio of $r = 0.3$ at both $\overline{T}_1$ and $\overline{T}_4$ as indicated in Fig. 16 of the supplementary information. The peak of the volume based 1D aspect ratio distribution (Fig. 13 of supplementary information) from Morphologi for metformin occurs at about 0.45 for the starting material. However, the corresponding estimate for the milled product shows a shoulder covering around 0.55–0.85. When this data is represented on number basis (Fig. 14 of supplementary information), the peaks of the estimated 1D aspect ratio distribution from Morphologi for metformin almost coincide at 0.75.

This situation occurs because the metformin sample contains a significant amount of fines as seen in Figs. 5 and 6 of the supplementary information. As the CLD modality is biased towards larger particles, which are more elongated in this case, the estimated aspect ratio of $r = 0.3$ at $\overline{T}_1$ is closer to the position of the peak of the 1D aspect ratio distribution from the Morphologi on volume basis rather than on number basis. This is because the smaller particles, which dominate the number based distribution, are more rounded than the larger particles.
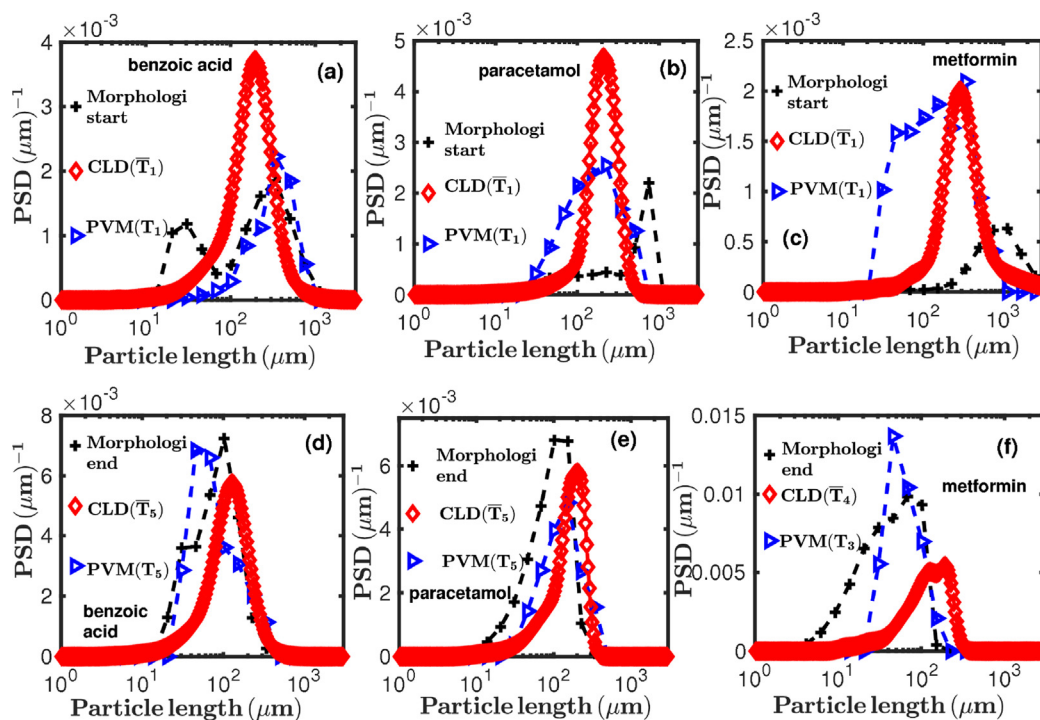
Fig. 5. The volume based PSDs (a)–(c) estimated for the starting materials using data from the offline Morphologi instrument, CLD analysis at $\overline{T}_1$, PVM image analysis at T_1 for each of the materials indicated. Similar estimates of the volume based PSDs at $T_3, \overline{T}_4, \overline{T}_5, T_5$, and for the milled products for each of the materials are shown in (d)–(e).

3.4.3. Limitations of inline image analysis

Analysis of images captured with inline instruments such as the PVM comes with a number of challenges. One issue is objects not being in the focal plane of the camera [19]. Even though the image processing algorithm used in this work has a focus threshold, which allows objects captured out of focus to be rejected, some of these objects still get accepted when they just meet the criteria used for acceptance. Similarly, some objects are only captured partially in focus, so that only a part of the object's boundary will be detected. The size and shape of these objects captured out of focus or partially in focus are not well represented in the data. This situation contributes to the aspect ratios estimated for the three samples at both T_1 and T_5 extending up to 1, as seen in Fig. 4(a) for benzoic acid, and in Figs. 11–14 of the supplementary information for paracetamol and metformin respectively. Another factor contributing to the aspect ratio distribution extending to 1 at both T_1 and T_5 is that the suspensions contained a significant amount of fines as seen in the PVM images in Figs. 7–9 of the supplementary information. These fines are mostly more rounded than the larger more elongated particles.

Another limitation of image analysis is the case of objects touching the edge of the image frame. These objects are rejected from the analysis. This leads to a situation where the estimated PSD from image analysis is biased towards smaller particles when there is a significant amount of large particles touching the image frame. This effect is more pronounced in the case of metformin at T_1, where the estimated volume based PSD from PVM images is shifted to the left of the corresponding estimate of the starting material of metformin obtained with the offline Morphologi instrument, as seen in Fig. 5(c). However, as mentioned earlier, it could also be that some of the long (with lengths ≈ 3000 μm) rod-like particles in the starting material of metformin may have broken to smaller particles upon suspension and agitation.

All images are affected by a resolution limit of the camera used, whereby small objects that are too close to the resolution limit are no longer distinguishable from the background noise of the image.

As these objects are removed from the analysis, the fines could become under estimated if there is a significant amount of small particles in suspension. This is the reason all the particle sizes estimated from PVM images in this work have a cut-off close to 25 μm as seen in Figs. 4 and 5, and similarly in Figs. 17–21 of the supplementary information. This effect is even more pronounced in the case of metformin where it was virtually impossible to see objects in the PVM images at T_4 (Fig. 9(T_4) of the supplementary information). Hence, analysis of images captured at T_4 for metformin was not done in this work. That is why the volume based PSD for metformin in Fig. 5(f) was estimated at T_3. This effect is also seen in the estimated relative mean number of objects per frame $\widehat{N}_{IMG}$. As the wet milling progresses, the number of objects detectable in images reduces due to the reduction in particle sizes, hence the value of $\widehat{N}_{IMG}$ shows a small decrease after an initial increase. This is seen in the case of metformin shown in Fig. 22 of the supplementary information.

Objects which overlap each other also pose a limitation to analysis of images. As the suspension density increases, the number of objects overlapping each other in the images increase. These overlapping objects give misleading estimates of size and shape. Some of these overlapping objects can be seen in the PVM images in Figs. 7–9 of the supplementary information. This issue of overlapping objects puts a limit on the suspension density in which analysis of inline images is applicable.

4. Effect of mill rotational speed on particle size

The results shown in the previous sections show an overall decrease in particle size as a result of the wet milling. This decrease is reflected in all the PSDs estimated from CLD and both inline and offline images. The decrease in particle size and corresponding increase in particle number is also reflected in the estimated mean number of objects per frame $\widehat{N}_{IMG}$ (from inline images) as a func-
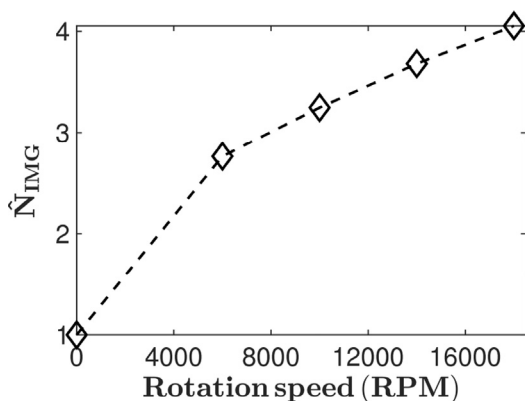
Fig. 6. The relative number of objects per frame $\widehat{N}_{IMG}$ estimated from the images captured with the inline PVM instrument over time covering the period T_1 to T_5 are shown by the symbols.

tion of rotation speed. This is shown in Fig. 6. This is similar to the situation observed in $\widehat{N}_{CLD}$ in Fig. 3(a).

In order to accurately capture the increasing number of smaller particles as rotational speed increases, we counted all objects in images rather than just those in focus, as the number of objects detected in focus reduce with decreasing size near the resolution limit (which is around 25 µm here). Taking only objects in focus would lead to a reduction of the mean number of objects per frame, although this may eventually happen if particles become too small to be resolved by the camera.

In Fig. 7 we can see the dependence of the volume weighted mean particle length D_{43} as a function of wet mill rotational speed, estimated from both CLD data and inline images, together with values from offline analysis estimated before and after milling. There is a good agreement between results from the two inline methods in all three cases. There is also a good agreement between inline and offline measurements.

In the case of metformin, the estimated D_{43} value of the starting material obtained from Morphologi is more than double the corresponding values from inline CLD and PVM. This is seen in Fig. 7(c). This is because of the long rod-like particles of order 3000 µm in the starting material of metformin. These particles were out of the range of measurements of FBRM and PVM as discussed earlier.

A similar situation is seen with paracetamol. The agglomerates present in the starting material of paracetamol (Fig. 3 of supplementary information) causes the estimated D_{43} value of the starting material to be about double of those of the estimates from inline CLD and PVM images at 0 rpm. This is seen in Fig. 7(b). Furthermore, the estimated D_{43} value of the milled product of paracetamol is about half the values estimated from inline CLD and PVM images. This could have been due to generation of fines during filtration and drying of the milled paracetamol.

Finally, we can also see that the mean particle size dependence on wet mill rotational speed between 6000 and 14,000 rpm is relatively gradual for both benzoic acid and paracetamol, while for metformin there is a very large decrease in the mean size after the lowest rotational speed (6000 rpm) is applied, followed by relatively little change afterwards. This indicates that material properties of crystals and solvents used are likely to play a significant role in performance of high shear wet mills in pharmaceutical manufacturing.

5. Conclusions

We have employed our recently developed computational tools for estimating particle size and shape distributions from inline CLD and imaging data to study changes in particle size, shape and number in slurries during wet milling with variation in milling speed. We have also compared the estimates from the inline instruments to corresponding estimates from offline analysis. The results show that these tools are suitable for monitoring changes in particle size and shape distributions and number of particles in slurries. The ability to capture changes in the quantitative particle attributes
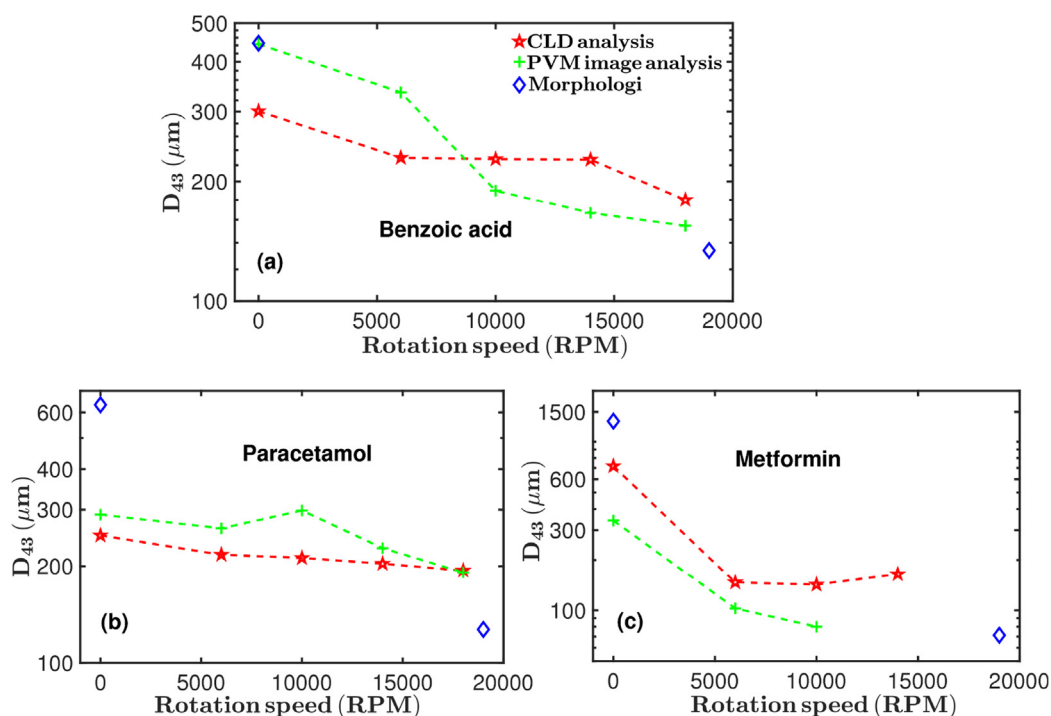

Fig. 7. Estimated D_{43} values of particle length for the three materials using the three modalities as indicated. The estimates from the offline Morphologi instrument are added just for comparison as the particles were not in suspension during the measurement.

show the promise these tools hold for aiding modelling and control of crystallisation processes. The quantitative PSD and shape information obtained inline and in real time can be used to tune kinetic parameters in population balance models for crystallisation processes, accounting for time dependence of kinetic process parameters.

However, some inconsistencies were observed between estimates from inline and offline measurements, and possible reasons for the discrepancies were discussed. Our results also reveal some of the challenges of estimating PSD from data captured with inline instruments. Inline imaging is limited to particles of certain minimum sizes due to camera resolution limits and out of focus rejection requirements for image processing algorithms. In addition, the PSD estimated by inline imaging becomes less representative as the sizes of the particles approach the size of the image frame. Similarly, the measured chord length from the FBRM sensor becomes less accurate as the length of needle-like particles approach the diameter of the circular trajectory of the FBRM laser spot. Also, CLD data could be affected by chords measured from bubbles present in the process. The CLD data could also become unrepresentative when there is significant chord splitting at the edges of the particles.

Approaches for combining both CLD and imaging data in a multi-objective optimisation approach are being explored in our further work in order to improve the robustness and accuracy of estimated PSD from inline CLD and imaging data.

Data management

All images captured with the PVM sensor as well as the data from the offline Morphologi instrument and CLD data from the FBRM sensor have been deposited in the publicly accessible repository.

Acknowledgement

Appendix A. Supplementary material

Supplementary data associated with this article can be found, in the online version, at https://doi.org/10.1016/j.apt.2018.09.003.

References

[1] P. Barrett, B. Smith, J. Worlitschek, V. Bracken, B. O' Sullivan, D. O' Grady, A review of the use of process analytical technology for the understanding and optimization of production batch crystallization processes, Org. Process Res. Dev. 9 (2005) 348–355.

[2] E.L. Paul, H.-H. Tung, M. Midler, Organic crystallization processes, Powder Technol. 150 (2005) 133–143.

[3] J. Chen, B. Sarma, J.M.B. Evans, A.S. Myerson, Pharmaceutical crystallization, Cryst. Growth Des. 11 (2011) 887–895.

[4] C.J. Brown, T. McGlone, S. Yerdelen, V. Srirambhatla, F. Mabbott, R. Gurung, M. L. Briuglia, B. Ahmed, H. Polyzois, J. McGinty, F. Perciballi, D. Fysikopoulos, P. MacFhionnghaile, H. Siddique, V. Raval, T.S. Harrington, A.D. Vassileiou, M. Robertson, E. Prasad, A. Johnston, B. Johnston, A. Nordon, J.S. Srai, G. Halbert, J. H. ter Horst, C.J. Price, C.D. Rielly, J. Sefcik, A.J. Florence, Enabling precision manufacturing of active pharmaceutical ingredients: workflow for seeded cooling continuous crystallisations, Mol. Syst. Des. Eng. 3 (2018) 518–549.

[5] H. Adi, I. Larson, P. Stewart, Use of milling and wet sieving to produce narrow particle size distributions of lactose monohydrate in the sub-sieve range, Powder Technol. 179 (2007) 95–99.

[6] T. Kamahara, M. Takasuga, H.H. Tung, K. Hanaki, T. Fukunaka, B. Izzo, J. Nakada, Y. Yabuki, Y. Kato, Generation of fine pharmaceutical particles via controlled secondary nucleation under high shear environment during crystallization - process development and scale-up, Org. Process Res. Dev. 11 (2007) 699–703.

[7] A. Harter, L. Schenck, I. Lee, A. Cote, High-shear rotor-stator wet milling for drug substances: expanding capability with improved scalability, Org. Process Res. Dev. 17 (2013) 1335–1344.

[8] Y. Yang, L. Song, T. Gao, Z.K. Nagy, Integrated upstream and downstream application of wet milling with continuous mixed suspension mixed product removal crystallization, Cryst. Growth Des. 15 (2015) 5879–5885.

[9] C.V. Luciani, E.W. Conder, K.D. Seibert, Modeling-aided scale-up of high-shear rotor-stator wet milling for pharmaceutical applications, Org. Process Res. Dev. 19 (2015) 582–589.

[10] Y. Yang, L. Song, Y. Zhang, Z.K. Nagy, Application of wet milling-based automated direct nucleation control in continuous cooling crystallization processes, Ind. Eng. Chem. Res. 55 (2016) 4987–4996.

[11] D. Acevedo, V.K. Kamaraju, B. Glennon, Z.K. Nagy, Modeling and characterization of an in situ wet mill operation, Org. Process Res. Dev. 21 (2017) 1069–1079.

[12] Y. Yang, K. Pal, A. Koswara, Q. Sun, Y. Zhang, J. Quon, R. Mckeown, C. Goss, Z.K. Nagy, Application of feedback control and in situ milling to improve particle size and shape in the crystallization of a slow growing needle-like active pharmaceutical ingredient, Int. J. Pharm. 533 (2017) 49–61.

[13] F. Salvatori, M. Mazzotti, Manipulation of particle morphology by crystallization, milling and heating cycles - a mathematical modeling approach, Ind. Eng. Chem. Res. 56 (2017) 9188–9201.

[14] B. Szilágyi, Z.K. Nagy, Population balance modeling and optimization of an integrated batch crystallizer-wet mill system for crystal size distribution control, Cryst. Growth Des. 18 (2018) 1415–1424.

[15] D. Wilson, M. Bunker, D. Milne, A. Jawor-Baczynska, K. Powell, J. Blyth, D. Streather, Particle engineering of needle shaped crystals by wet milling and temperature cycling: optimisation for roller compaction, Powder Technol. 339 (2018) 641–650.

[16] J. Heinrich, J. Ulrich, Application of laser-backscattering instruments for in situ monitoring of crystallization processes - a review, Chem. Eng. Technol. 35 (6) (2012) 967–979.

[17] A. Vaccaro, J. Sefcik, M. Morbidelli, Modeling focused beam reflectance measurement and its application to sizing of particles of variable shape, Part. Part. Syst. Charact. 23 (2007) 360–373.

[18] O.S. Agimelen, P. Hamilton, I. Haley, A. Nordon, M. Vasile, J. Sefcik, A.J. Mulholland, Estimation of particle size distribution and aspect ratio of non-spherical particles from chord length distribution, Chem. Eng. Sci. 123 (2015) 629–640.

[19] O.S. Agimelen, A. Jawor-Baczynska, J. McGinty, J. Dziewierz, C. Tachtatzis, A. Cleary, I. Haley, C. Michie, I. Andonovic, J. Sefcik, A.J. Mulholland, Integration of in situ imaging and chord length distribution measurements for estimation of particle size and shape, Chem. Eng. Sci. 144 (2016) 87–100.

[20] J. Cardona, C. Ferreira, J. McGinty, A. Hamilton, O.S. Agimelen, A. Cleary, R. Atkinson, C. Michie, S. Marshall, Y.-C. Chen, J. Sefcik, I. Andonovic, C. Tachtatzis, Image analysis framework with focus evaluation for in situ characterisation of particle size and shape attributes, Chem. Eng. Sci. 191 (2018) 208–231.

[21] M. Li, D. Wilkinson, Determination of non-spherical particle size distribution from chord length measurements. Part 1: theoretical analysis, Chem. Eng. Sci. 60 (2005) 3251–3265.

[22] O.S. Agimelen, A.J. Mulholland, J. Sefcik, Software for transforming measured chord length distribution data to particle size distribution, 2018. <https://doi.org/10.15129/c147b4c4-6e2e-43bd-bdfd-fd889ef2d5ee>.

[23] J. Cardona, C. Tachtatzis, Image analysis software for particle size and shape characterisation, 2018. <https://doi.org/10.15129/99c4558f-f59e-4be8-80e2-b0425178332b>.

[24] N. Kail, H. Briesen, W. Marquardt, Advanced geometrical modeling of focused beam reflectance measurements (FBRM), Part. Part. Syst. Charact. 24 (2007) 184–192.

[25] N. Kail, W. Marquardt, H. Briesen, Estimation of particle size distributions from focused beam reflectance measurements based on an optical model, Chem. Eng. Sci. 64 (2009) 984–1000.